Journal of Alloys and Compounds 509 (2011) 3080–3088

Contents lists available at ScienceDirect

Journal of Alloys and Compounds

journal homepage: www.elsevier.com/locate/jallcom

Thermodynamic assessment of the Nb–Ge system

Tai Geng[a], Changrong Li[a,*], Zhenmin Du[a], Cuiping Guo[a], Xinqing Zhao[b], Huibin Xu[b]

[a] School of Materials Science and Engineering, University of Science and Technology Beijing, Xueyuan Road, 30#, Haidian District, Beijing 100083, PR China
[b] School of Materials Science and Engineering, Beijing University of Aeronautics and Astronautics, Beijing 100083, PR China

ARTICLE INFO

Article history:
Received 10 December 2009
Accepted 2 December 2010
Available online 9 December 2010

Keywords:
Nb–Ge phase diagram
Thermodynamic properties
CALPHAD technique

ABSTRACT

The Nb–Ge binary system has been thermodynamically assessed using the CALPHAD (Calculation of Phase Diagrams) approach on the basis of the experimental data of both the phase equilibria and the thermochemical properties. The reasonable models were constructed for all the phases of the system. The liquid and the terminal solid solution phases, Bcc-(Nb) and Diamond-(Ge), were described as the substitutional solutions with Redlich–Kister polynomials for the expressions of the excess Gibbs free energies. The intermediate phases (Nb_3Ge), (Nb_5Ge_3), (Nb_3Ge_2) and ($NbGe_2$) with homogeneity ranges were treated as the sublattice models $Nb_{0.75}(Ge,Nb,Va)_{0.25}$, $Nb_{0.5}(Nb,Ge)_{0.125}(Ge,Va)_{0.375}$, $(Nb,Ge)_{0.222}(Nb,Ge)_{0.333}Nb_{0.333}(Ge,Va)_{0.111}$ and $(Nb,Ge)_{0.333}(Nb,Ge)_{0.667}$ respectively based on their structure features of atom arrangements. A set of self-consistent thermodynamic parameters for the Nb–Ge system was obtained. Using the present thermodynamic data, the calculation results can reproduce the experimental data well.

1. Introduction

The compounds of the Nb–Ge system have been focused into many applications due to their special physical and chemical properties. For example, the Nb–Ge superconducting films made of the Nb_3Ge phase with A15 crystalline structure process excellent superconducting critical properties, such as high critical temperature (T_c), upper critical field (H_c) and high current carrying capacity [1–4]. The Nb_5Ge_3 compound with the composition M_5X_3 (M = Mo, Nb and Ti transition metals, and X = Si and Ge semimetallic elements) can exhibit extremely high thermal stability and can be used as the candidate of high-temperature materials [5,6]. Understanding the phase equilibria as well as the thermochemical behavior of the system is helpful for the development of the related materials. The Nb–Ge system has not been thermodynamically assessed because of the limited thermodynamic data and the different arguments on whether the Nb_3Ge_2 phase can exist or not as a stable phase in the Nb–Ge phase diagram. The present paper deals with an assessment of the thermodynamic description of the Nb–Ge system with the inclusion of the newly confirmed stable phase Nb_3Ge_2 by means of the CALPHAD (Calculation of Phase Diagram) technique and provides a set of self-consistent parameters for calculation of phase equilibria and thermochemical properties of the system.

2. Experimental

2.1. Phase equilibria

The complete investigation of the Nb–Ge phase diagram was originally measured by Pan et al. [7], including four intermediate compounds (Nb_3Ge), (Nb_5Ge_3), (Nb_3Ge_2) and ($NbGe_2$) with homogeneity ranges, two terminal solution phases Bcc-(Nb) and Diamond-(Ge), two eutectic reactions and three peritectic reactions. Muller [8] gave a partial phase diagram of the Nb–Ge system at Nb-rich side in the temperature range from 1600 to 2065 °C. Jorda et al. [9] later reinvestigated a majority of the Nb–Ge equilibrium phase diagram by means of X-ray diffraction (XRD), metallography, hardness measurements, microprobe analysis and differential thermal analysis (DTA) up to 2200 °C. For temperatures higher than 1870 °C, the solidus lines were determined by thermal analysis on levitating samples. To obtain high accuracy of the Nb–Ge phase diagram, the weight losses during the melting were also compensated due to the vaporization of Ge at higher concentrations than 30 at.%. Feschotte et al. [10] measured and estimated the homogeneity ranges of the phases in the Nb–Ge phase diagram in the temperature range from 600 to 1050 °C and also determined the temperatures of the eutectic reactions L ↔ (Nb_5Ge_3) + ($NbGe_2$) at 1593 °C and L ↔ ($NbGe_2$) + Diamond-(Ge) at 937 °C respectively. The phase Nb_3Ge_2 has not been suggested in both Refs. [9,10].

The solubility of Ge in Bcc-(Nb) measured by Jorda et al. [9] increases from 4 ± 1 to 11.5 ± 1 at.% Ge within the temperature range from 1000 to 1900 °C, which is higher than that of 2–8 at.% Ge determined by Pan et al. [7] and that of 3–5% at.% Ge by Muller [8]. The (Nb_3Ge) phase is formed by a peritectic reaction L + Bcc-(Nb) ↔ (Nb_3Ge), which is measured at 1900 ± 10 °C, 18 ± 1 at.% Ge by Jorda et al. [9], at 1970 °C, 18 at.% Ge by Pan et al. [7] and at 1910 °C, 18 at.% Ge by Muller [8]. The homogeneity range of the (Nb_3Ge) phase was confirmed between 18–23 at.% Ge by Jorda et al. [9], 15–18 at.% Ge by Pan et al. [7] and 18–19 at.% Ge by Muller [8]. The eutectic reaction L ↔ (Nb_3Ge) + (Nb_5Ge_3) occurs at 1865 °C, 27 at.% Ge measured by Jorda et al. [9], (1930 °C, 26 at.% Ge) by Pan et al. [7] and 1900 °C, 21.8 at.% Ge by Muller [8]. The congruent melting point of (Nb_5Ge_3) measured by Jorda et al. [9] is 2180 ± 10 °C which is higher than that of 2150 °C by Pan et al. [7] and 2065 °C by Muller [8], and the homogeneity range of (Nb_5Ge_3) extends from 38 to 44 at.% Ge [9] which is distinctly different from the range (34–36 at.% Ge) given by Pan

* Corresponding author. Tel.: +86 10 6233 3607.
E-mail address: crli@mater.ustb.edu.cn (C. Li).

0925-8388/$ – see front matter © 2010 Elsevier B.V. All rights reserved.
doi:10.1016/j.jallcom.2010.12.005

Table 1
The experimental data of the Nb–Ge system.

Reaction	Composition (at.% Ge)			T (°C)	Method	Reaction-type	Reference
L + Bcc-(Nb) ↔ (Nb_3Ge)	19	8	18	1970	Experiment	Peritectic	[7]
	18.5	4	18.3	1910	Experiment	Peritectic	[8]
	22 ± 1	11.5 ± 1	18 ± 1	1900 ± 10	Experiment	Peritectic	[9]
	22	11.5	18	1900	Evaluated	Peritectic	[11]
	22	11.1	18.1	1903	Calculated	Peritectic	This work
L ↔ (Nb_3Ge) + (Nb_5Ge_3)	26.5	20	33.4	1930	Experiment	Eutectic	[7]
	21.8	18.8	36.1	1900	Experiment	Eutectic	[8]
	27	23 ± 1	37.1	1865 ± 5	Experiment	Eutectic	[9]
	27	23	36.5	1865	Evaluated	Eutectic	[11]
	25	24	37	1865	Calculated	Eutectic	This work
L ↔ (Nb_5Ge_3)	35.7	35.7		2150	Experiment	Congruent	[7]
	38.4	38.4		2065	Experiment	Congruent	[8]
	38.0	38.0		2180 ± 10	Experiment	Congruent	[9]
	37	37		2180	Evaluated	Congruent	[11]
	38.2	38.2		2179	Calculated	Congruent	This work
L ↔ (Nb_3Ge_2) + ($NbGe_2$)	60	44.4	66.8	1590	Experiment	Eutectic	[7]
	58	43	66	1589.4	Calculated	Eutectic	This work
L ↔ (Nb_5Ge_3) + ($NbGe_2$)	–	–	–	1590	Experiment	Eutectic	[10]
	59.2	44.4	66.2	1580 ± 10	Experiment	Eutectic	[9]
	58	43	66	1589.4	Evaluated	Eutectic	[11]
L ↔ ($NbGe_2$)	67.0	67.0		1680	Experiment	Congruent	[7]
	66.5	66.5		1680	Experiment	Congruent	[9]
	66.1	66.1		1680	Evaluated	Congruent	[11]
	66.7	66.7		1680	Calculated	Congruent	This work
L ↔ ($NbGe_2$) + Diamond-(Ge)	~100	67.4	99.9	937	Experiment	Eutectic	[10]
	99.5	67.2	99.7	937.8	Calculated	Eutectic	This work
L + ($NbGe_2$) ↔ Diamond-(Ge)	~100	68.7	99.9	950	Experiment	Peritectic	[7]
	~100	68.7	99.9	950	Evaluated	Peritectic	[11]
L + (Nb_5Ge_3) ↔ (Nb_3Ge_2)	45.7	35.7	40.9	2040	Experiment	Peritectic	[7]
	46.8	39.3	41	2040	Calculated	Peritectic	This work

et al. [7] and the range (37.5–42.3 at.% Ge) given by Feschotte et al. [10]. The eutectic reaction L ↔ Nb_5Ge_3 + $NbGe_2$ was measured at 1580 ± 10 °C, 59 at.% Ge by Jorda et al. [9], at 1590 °C, 60 at.% Ge by Pan et al. [7] and at 1590 °C by Feschotte et al. [10]. The congruent melting point of ($NbGe_2$) is 1680 °C [9]. For a same isothermal reaction, the peritectic reaction L + $NbGe_2$ ↔ Diamond-(Ge) was measured at 950 °C by Pan et al. [7] while the eutectic reaction L ↔ $NbGe_2$ + Diamond-(Ge) was proposed at 937 °C by Feschotte et al. [10].

Okamoto [11] reviewed the literature data and constructed the Nb–Ge phase diagram which is mainly based on the experimental results measured by Jorda et al. [9] and Pan et al. [7].

The experimental data and the crystalline structures of the different phases in the Nb–Ge system are shown in Tables 1 and 2 respectively.

2.2. The existence of the phase Nb_3Ge_2

The phase Nb_3Ge_2 is also known as hexagonal Nb_5Ge_3, β-Nb_5Ge_3, $Nb_{10}Ge_7$, $NbGe_{0.67}$ or $Nb_5Ge_{3.5}$ and crystallizes in the Mn_5Si_3 prototype ($D8_8$) with the space group $P6_3/mcm$ (No. 193). This phase with the hexagonal Mn_5Si_3 structure is usually regarded as a metastable phase and can be easily stabilized by the interstitial elements like B, C, N, O [13–15], which occupy the 2b sites of the space lattice.

Corbett et al. [16] pointed out that only some phases with the hexagonal Mn_5Si_3 structure require interstitial stabilization, while others can well be prepared under clean conditions. Nowotny et al. [17] firstly reported the existence of the Nb_3Ge_2 with the composition of $NbGe_{0.67\pm0.5}$. Braginski et al. [18] and Iijima et al. [19] later detected different ranges of Nb_3Ge_2 by chemical vapor deposition and diffusion couples respectively.

Pan et al. [7] and Jorda et al. [9] presented two different Nb–Ge phase diagrams. Pan et al. [7] testified that the phase Nb_3Ge_2 appears from a peritectic reaction L + Nb_5Ge_3 ↔ NB_3Ge_2 at 41 at.% Ge, 2040 °C, while Jorda et al. [9] claimed that this hexagonal Mn_5Si_3-type phase was impurity stabilized and excluded it from the Nb–Ge phase diagram.

Kloska and Haase [20] discussed the existence of the hexagonal Nb_3Ge_2 phase based on literatures and prepared thin films with a composition near Nb_3Ge_2 under clean conditions. A new phase with two different characteristic X-ray pulses compared with that of Nb_3Ge_2 was found. They believed that the phase Nb_3Ge_2 was either stabilized by light elements or metastable. This thin film phase can also be stabilized by substrate since the lattice epitaxial growth.

Recently, Richter et al. [21] studied the alloys around the composition 34–50 at.% Ge at temperatures between 1100 and 1350 °C using X-ray powder diffraction and electron probe microanalysis. They conquered the influence of the impurity atoms and oxidation of the samples and believed that the Nb_3Ge_2 was formed as a binary stable phase. The homogeneity range of (Nb_3Ge_2) is 41.6–42 at.% Ge at 1100 °C. The Ge contents of the Nb_3Ge_2 phase of different literatures are shown in Table 3.

In the present assessment work, the experimental information of the phase Nb_3Ge_2 is taken from Pan et al. [7] and Richter et al. [21].

2.3. Thermochemical data

Carpenter [22] calculated the enthalpy of the decomposition reaction $6.67NbGe_{0.15}(s) \leftrightarrow 6.67Nb(s) + Ge(g)$ at 25 °C and reported the enthalpy of Nb_3Ge compound with a composition of $NbGe_{0.15}$. Later Carpenter and Searcy [23] calculated the enthalpies of Nb_5Ge_3, Nb_3Ge_2 and $NbGe_2$ with the composition $NbGe_{0.54}$, $NbGe_{0.67}$ and $NbGe_2$ at 25 °C respectively in the same way as Ref. [22]. Wan and

Table 2
The structure information of Nb–Ge system.

Phase	Pearson symbol	Space group	Struk designation	Prototype	Structure description	Reference
Bcc-(Nb)	cI2	$Im\bar{3}m$	A2	W	Body-centered cubic	[9,12]
(Nb_3Ge)	cP8	$Pm\bar{3}n$	A15	Cr_3Si	Cubic	[9,11,12]
(Nb_5Ge_3)	tI32	$I4/mcm$	$D8_m$	W_5Si_3	Tetragonal	[9,11,12]
(Nb_3Ge_2)	hP16	$P6_3/mcm$	$D8_8$	Mn_5Si_3	Hexagonal	[12,20,21]
($NbGe_2$)	hP9	$P6_222$	C40	$CrSi_2$	Hexagonal	[9,11,12]
Diamond-(Ge)	cF8	$Fd\bar{3}m$	A4	C(Diamond)	Diamond	[12]

Table 3
The content of the Nb_3Ge_2 ($D8_8$) phase (at.% Ge).

The range of the composition	Method	Reference
40–43	Microprobe analysis	[7]
38.3–41.9	Chemical vapor deposition	[18]
41.8–43.7	Diffusion couples	[19]
40–44	Co-evaporation	[20]
41.6–42	Microprobe analysis at 1100 °C	[21]
41–43	CALPHAD	This work

Spear [24] estimated the approximations of the enthalpies and entropies at 927 °C for the compounds of $NbGe_{0.33}$, $NbGe_{0.54}$, $NbGe_{0.67}$ and $NbGe_2$. deBoer et al. [25] calculated the enthalpies of all the intermediate compounds in the Nb–Ge phase diagram. Beloborodova [26] measured the formation enthalpy and the mix enthalpy of the liquid phase in the composition range of 80–100 at.% Ge at 1700 °C.

3. Thermodynamic models

3.1. Unary phase

The Gibbs free energy function ${}^0G_i^\varphi(T) = G_i^\varphi(T) - H_i^{SER}$ (298.15 K) for the pure element i (i = Nb or Ge) in the structure of phase φ (φ = Bcc-(Nb), Diamond-(Ge) and Liquid) is described by a function of temperature as follows:

$$
\begin{aligned}
{}^0G_i^\varphi(T) &= G_i^\varphi(T) - H_i^{SER} \quad (298.15\ \text{K}) \\
&= a + bT + cT \ \ln\ T + dT^2 + eT^3 + fT^{-1} + gT^7 + hT^{-9} \qquad (1)
\end{aligned}
$$

where H_i^{SER} (298.15 K) is the molar enthalpy of the element i in its stable element reference (SER) state at 298.15 K and 101.325 Pa, T is the absolute temperature, and a, b, c, d, e, f, g and h are coefficients. The Gibbs free energy of the element i in its SER state, ${}^0G_i^\varphi(T)$, is denoted by $GHSER_i$.

$$GHSER_{Nb} = G_{Nb}^{Bcc}(T) - H_{Nb}^{SER} \quad (298.15) \qquad (2)$$

$$GHSER_{Ge} = G_{Ge}^{Diamond}(T) - H_{Ge}^{SER} \quad (298.15) \qquad (3)$$

The Gibbs free energy functions for the pure elements Nb and Ge are taken from the compiled data by Dinsdale [27] in the present work.

3.2. Solution phases Liquid, Bcc-(Nb), and Diamond-(Ge)

The substitutional solution model was chosen for the Liquid, Bcc-(Nb) and Diamond-(Ge) phases. The molar Gibbs free energy is expressed as follows:

$$G_m^\varphi = x_{Ge}^\varphi\, {}^0G_{Ge}^\varphi + x_{Nb}^\varphi\, {}^0G_{Nb}^\varphi + RT(x_{Ge}^\varphi\ \ln x_{Ge}^\varphi + x_{Nb}^\varphi\ \ln x_{Nb}^\varphi) + {}^EG_m^\varphi \qquad (4)$$

where ${}^EG_m^\varphi$ is the excess Gibbs free energy and is written as a Redlich–Kister polynomial:

$$ {}^EG_m^\varphi = x_{Ge}^\varphi x_{Nb}^\varphi \sum_{n=0}^{m} {}^nL_{Ge,Nb}^\varphi (x_{Ge}^\varphi - x_{Nb}^\varphi)^n \qquad (5)$$

where ${}^nL_{Ge,Nb}^\varphi$ is the interaction parameter between Ge and Nb and is the function of temperature:

$${}^nL_{Ge,Nb}^\varphi = a + bT + cT \ \ln(T) + dT^2 + eT^{-1} + fT^3 + gT^7 + hT^{-9} \qquad (6)$$

where a, b, c, d, e, f, g and h are the coefficients to be optimized. In most cases, only the first one or two terms of the above equation are used.

3.3. Intermediate phases with solubility ranges

There are four nonstoichiometric compounds (Nb_3Ge_2), (Nb_5Ge_3), (Nb_3Ge) and ($NbGe_2$) with different homogeneity ranges.

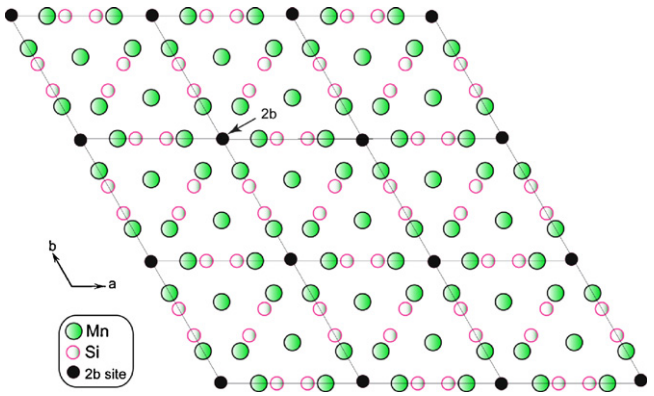

Fig. 1. Structure of Mn_5Si_3, view along [0 0 1].

Considering their crystal structures as listed in Table 2, the Gibbs free energies of the nonstoichiometric compounds are described by different sublattice models as follows.

3.3.1. (Nb_3Ge_2) phase

The phase Nb_3Ge_2 crystallizes in the Mn_5Si_3 prototype ($D8_8$) as shown in Fig. 1. In the crystal structure of the phase Nb_3Ge_2, the Ge atoms occupying the 2b sites cause the existence of Nb_3Ge_2 at the higher composition range than the stoichiometry 5:3 of its prototype Mn_5Si_3. Four kinds of atoms are located in the unit cell: Nb(1) (6g) at (1/4, 0, 1/4), Nb(2) (4d) at (1/3, 2/3, 0), Ge(1) (6g) at

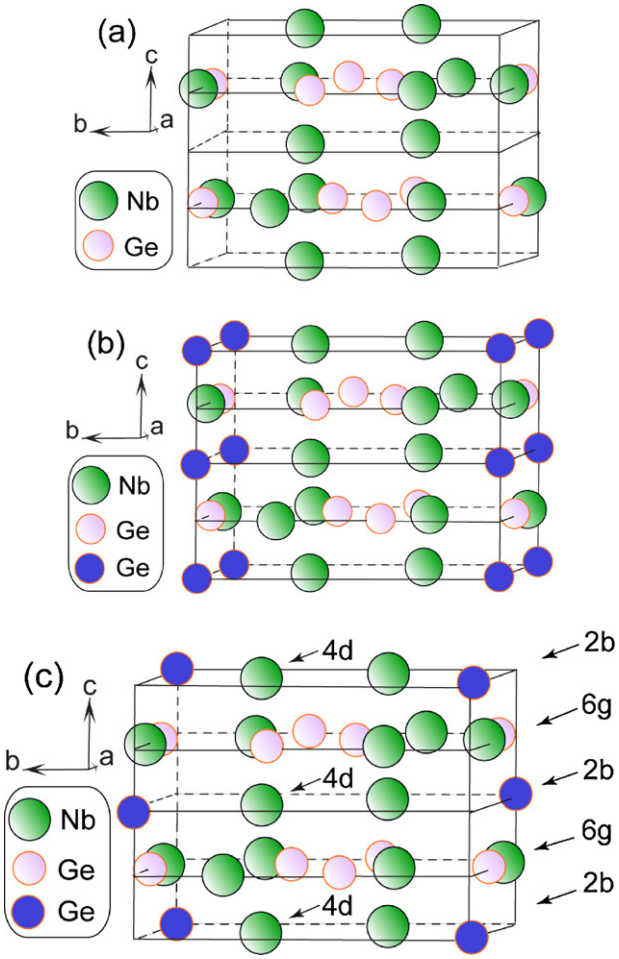

Fig. 2. Nb_3Ge_2-$D8_8$ structure. (a) No 2b sites occupied by Ge atoms; (b) all 2b sites occupied by Ge atoms; (c) partial 2b sites occupied by Ge atoms.

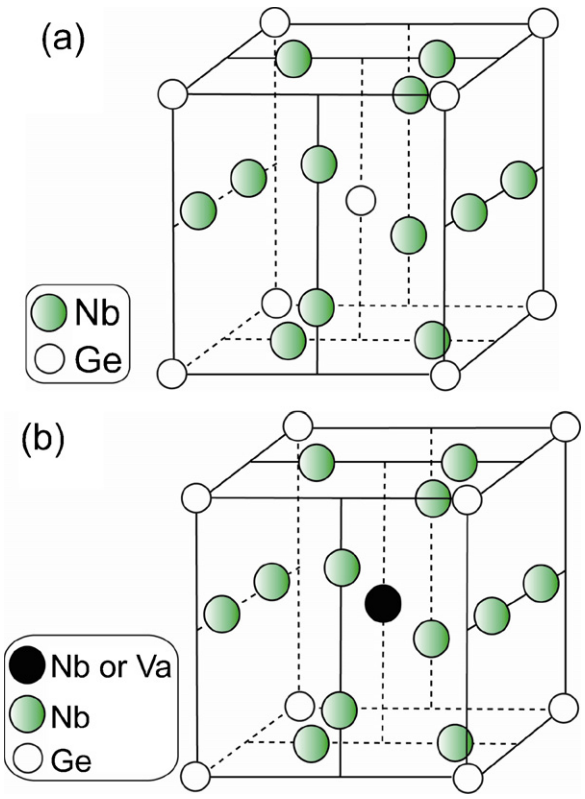

Fig. 3. Nb_3Ge-A15 structure. (a) X = 25 at.% Ge; (b) X < 25 at.% Ge.

(0.615, 0, 1/4), and Ge(2) (2b) at (0, 0, 0). A gradual transition from 5:3 (37.5 at.% Ge), Fig. 2a, to 5:4 (44.4 at.% Ge), Fig. 2b, will take place with increasing the occupancy of the 2b sites by Ge atoms. Fig. 2c shows the partial occupation of the 2b sites by Ge atoms.

Both (Nb_3Ge_2) and (Ti_5Si_3) phases are known to be of the same structure as the Mn_5Si_3-type ($D8_8$). Referring to the sublattice model of the (Ti_5Si_3) phase used by Seifert et al. [28], four sublattices $(Ge,Nb\%)_{0.222}(Ge\%,Nb)_{0.333}(Nb)_{0.333}(Ge,Va)_{0.111}$ are used to describe the Nb_3Ge_2 phase in the present work, with '%' representing the major component in the related sublattice. The Gibbs free energy of Nb_3Ge_2 is expressed as follows:

$$G_m^{(Nb_3Ge_2)} = {}^{ref}G_m^{(Nb_3Ge_2)} + {}^{id}G_m^{(Nb_3Ge_2)} + {}^{ex}G_m^{(Nb_3Ge_2)} \quad (7)$$

$$\begin{aligned} {}^{ref}G_m^{(Nb_3Ge_2)} = {} & y_{Ge}^{I} y_{Ge}^{II} y_{Ge}^{IV}\, {}^{0}G_{Ge:Ge:Nb:Ge}^{(Nb_3Ge_2)} + y_{Ge}^{I} y_{Ge}^{II} y_{Va}^{IV}\, {}^{0}G_{Ge:Ge:Nb:Va}^{(Nb_3Ge_2)} \\ & + y_{Ge}^{I} y_{Nb}^{II} y_{Ge}^{IV}\, {}^{0}G_{Ge:Nb:Nb:Ge}^{(Nb_3Ge_2)} + y_{Ge}^{I} y_{Nb}^{II} y_{Va}^{IV}\, {}^{0}G_{Ge:Nb:Nb:Va}^{(Nb_3Ge_2)} \\ & + y_{Nb}^{I} y_{Ge}^{II} y_{Ge}^{IV}\, {}^{0}G_{Nb:Ge:Nb:Ge}^{(Nb_3Ge_2)} + y_{Nb}^{I} y_{Ge}^{II} y_{Va}^{IV}\, {}^{0}G_{Nb:Ge:Nb:Va}^{(Nb_3Ge_2)} \\ & + y_{Nb}^{I} y_{Nb}^{II} y_{Ge}^{IV}\, {}^{0}G_{Nb:Nb:Nb:Ge}^{(Nb_3Ge_2)} + y_{Nb}^{I} y_{Nb}^{II} y_{Va}^{IV}\, {}^{0}G_{Nb:Nb:Nb:Va}^{(Nb_3Ge_2)} \end{aligned} \quad (8)$$

$$\begin{aligned} {}^{id}G_m^{(Nb_3Ge_2)} = {} & 0.222RT(y_{Ge}^{I} \ \ln \ y_{Ge}^{I} + y_{Nb}^{I} \ \ln \ y_{Nb}^{I}) \\ & + 0.333RT(y_{Ge}^{II} \ \ln \ y_{Ge}^{II} + y_{Nb}^{II} \ \ln \ y_{Nb}^{II}) \\ & + 0.111RT(y_{Ge}^{IV} \ \ln \ y_{Ge}^{IV} + y_{Va}^{IV} \ \ln \ y_{Va}^{IV}) \end{aligned} \quad (9)$$

$$\begin{aligned} {}^{ex}G_m^{(Nb_3Ge_2)} = {} & \sum_{i=Ge,Nb} \sum_{k=Ge,Va} y_{Ge}^{I} y_{Nb}^{I} y_i^{II} y_k^{IV}\, {}^{0}L_{Ge,Nb:i:Nb:k}^{(Nb_3Ge_2)} \\ & + \sum_{i=Ge,Nb} \sum_{k=Ge,Va} y_i^{I} y_{Ge}^{II} y_{Nb}^{II} y_k^{IV}\, {}^{0}L_{i:Ge,Nb:Nb:k}^{(Nb_3Ge_2)} \\ & + \sum_{i=Ge,Nb} \sum_{j=Ge,Nb} y_i^{I} y_j^{II} y_{Ge}^{IV} y_{Va}^{IV}\, {}^{0}L_{i:j:Nb:Ge,Va}^{(Nb_3Ge_2)} \end{aligned} \quad (10)$$

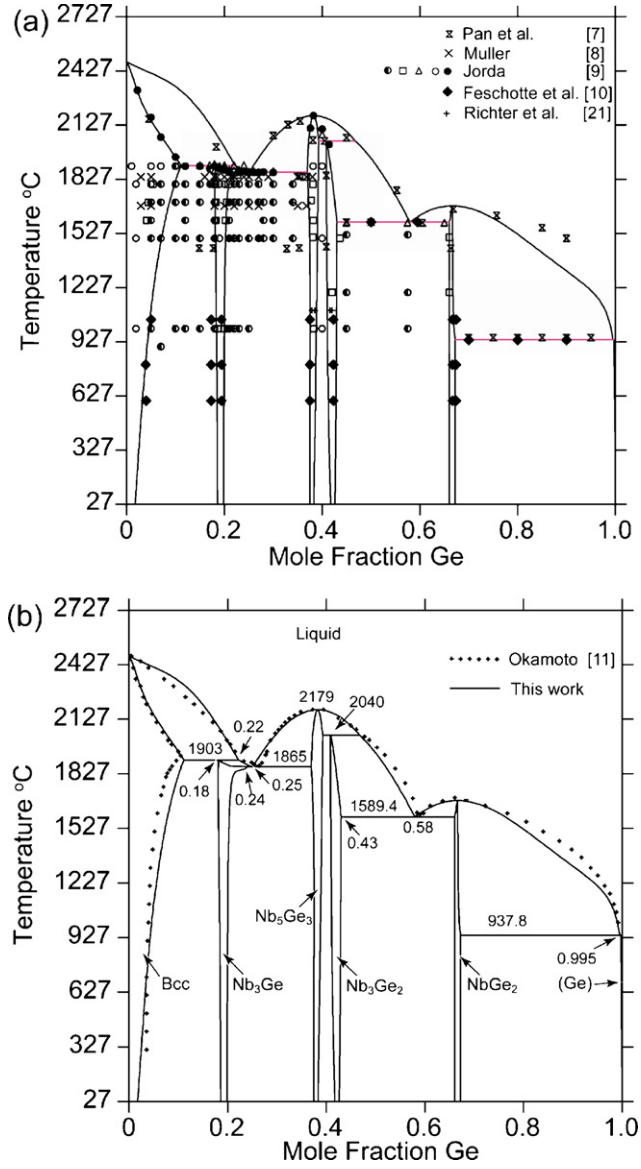

Fig. 4. The Nb–Ge phase diagram. (a) Optimized phase diagram and experimental data; (b) optimized phase diagram. The dotted line represents the liquids and the boundary of the solubility of Bcc-(Nb) evaluated by Okamoto [11].

$${}^{0}L_{Ge,Nb:i:Nb:k}^{(Nb_3Ge_2)} = \sum_{n=0} (a_n + b_n T)(y_{Ge}^{I} - y_{Nb}^{I})^n \quad (11a)$$

$${}^{0}L_{i:Ge,Nb:Nb:k}^{(Nb_3Ge_2)} = \sum_{n=0} (a_n + b_n T)(y_{Ge}^{II} - y_{Nb}^{II})^n \quad (11b)$$

$${}^{0}L_{i:j:Nb:Ge,Va}^{(Nb_3Ge_2)} = \sum_{n=0} (a_n + b_n T)(y_{Ge}^{IV} - y_{Va}^{IV})^n \quad (11c)$$

where ${}^{ref}G_m^{\varphi}$ represents the mechanical mixture energy of the hypothetical end member compounds; ${}^{id}G_m^{\varphi}$ the Gibbs free energy contribution by the ideal entropy of mixing; ${}^{ex}G_m^{\varphi}$ the excess Gibbs free energy; ${}^{0}G_{A:B:Nb:C}^{(Nb_3Ge_2)}$ (A, B = Ge, Nb and C = Ge, Va) the Gibbs free energy of the hypothetical end member compound $A_{0.222}B_{0.333}Nb_{0.333}C_{0.111}$. y_i^{I}, y_j^{II} and y_k^{IV} (i, j = Ge, Nb and k = Ge, Va) are the site fractions of components i, j and k in the 1st, 2nd and 4th sublattices respectively. To reduce the number of the

parameters of the Gibbs free energy expression, it is supposed that ${}^{0}L^{(Nb_3Ge_2)}_{Ge,Nb:Ge:Nb:k} = {}^{0}L^{(Nb_3Ge_2)}_{Ge,Nb:Nb:Nb:k}$, ${}^{0}L^{(Nb_3Ge_2)}_{Ge:Ge,Nb:Nb:k} = {}^{0}L^{(Nb_3Ge_2)}_{Nb:Ge,Nb:Nb:k}$, ${}^{0}L^{(Nb_3Ge_2)}_{i:Nb:Nb:Ge,Va} = {}^{0}L^{(Nb_3Ge_2)}_{i:Ge:Nb:Ge,Va}$ and ${}^{0}L^{(Nb_3Ge_2)}_{Nb:j:Nb:Ge,Va} = {}^{0}L^{(Nb_3Ge_2)}_{Ge:j:Nb:Ge,Va}$ in the present work. The parameters a_n and b_n are to be optimized.

In Eq. (8), the Gibbs free energy of formation of the hypothetical compound, ${}^{0}G^{(Nb_3Ge_2)}_{A:B:Nb:C}$, is expressed as follows:

$${}^{0}G^{(Nb_3Ge_2)}_{A:B:Nb:C} = a + bT + CT \quad \ln(T) + dT^2 + eT^{-1} + fT^3 + gT^7 + hT^{-9} \qquad (12)$$

where a, b, c, d, e, f, g and h are the parameters to be optimized.

3.3.2. (Nb_5Ge_3) phase

The (Nb_5Ge_3) phase is of the same structure as the (Nb_5Si_3) phase with the W_5Si_3-type ($D8_m$). Considering the similarity between Ge and Si, and referring to the three-sublattice model used by Fernandes et al. [29] to describe the (Nb_5Si_3) phase, the (Nb_5Ge_3) phase is modeled as $(Nb)_{0.5}(Ge,Nb\%)_{0.125}(Ge\%,Va)_{0.375}$ in the present optimization. Some vacancies are introduced in the 3rd sublattice to replace the Ge atoms since the homogeneity range of the phase (Nb_5Ge_3) spans both sides of the stoichiometric composition 37.5 at.% Ge [9]. The Gibbs free energy is given by the following expression.

$$\begin{aligned} G_m^{(Nb_5Ge_3)} = {} & y^{II}_{Ge} y^{III}_{Ge} {}^{0}G^{(Nb_5Ge_3)}_{Nb:Ge:Ge} + y^{II}_{Ge} y^{III}_{Va} {}^{0}G^{(Nb_5Ge_3)}_{Nb:Ge:Va} + y^{II}_{Nb} y^{III}_{Ge} {}^{0}G^{(Nb_5Ge_3)}_{Nb:Nb:Ge} \\ & + y^{II}_{Nb} y^{III}_{Va} {}^{0}G^{(Nb_5Ge_3)}_{Nb:Nb:Va} + 0.125RT(y^{II}_{Ge} \ln y^{II}_{Ge} + y^{II}_{Nb} \ln y^{II}_{Nb}) \\ & + 0.375RT(y^{III}_{Ge} \ln y^{III}_{Ge} + y^{III}_{Va} \ln y^{III}_{Va}) \\ & + \sum_{k=Ge,Va} y^{II}_{Ge} y^{II}_{Nb} y^{III}_{k} {}^{0}L^{(Nb_5Ge_3)}_{Nb:Ge,Nb:k} \\ & + \sum_{i=Ge,Nb} y^{II}_{i} y^{III}_{Ge} y^{III}_{Va} {}^{0}L^{(Nb_5Ge_3)}_{Nb:i:Ge,Va} \end{aligned} \qquad (13)$$

where y^{II}_i and y^{III}_k (i = Ge, Nb and k = Ge, Va) are the site fractions of components i and k in the 2nd and 3rd sublattices respectively. ${}^{0}G^{(Nb_5Ge_3)}_{Nb:A:B}$ (A = Nb, Ge and B = Ge, Va) represents the Gibbs free energy of the hypothetical end member compound $Nb_{0.5}A_{0.125}B_{0.375}$. To reduce the number of the Gibbs free energy expression, it is supposed that ${}^{0}L^{(Nb_5Ge_3)}_{Nb:Nb,Ge:Ge} = {}^{0}L^{(Nb_5Ge_3)}_{Nb:Nb,Ge:Va}$ and ${}^{0}L^{(Nb_5Ge_3)}_{Nb:Nb:Ge,Va} = {}^{0}L^{(Nb_5Ge_3)}_{Nb:Ge:Ge,Va}$ in the present work.

3.3.3. (Nb_3Ge) phase

The phase Nb_3Ge with Cr_3Si-type structure exhibits a considerable range of homogeneity on the Nb-rich side of the composition 18–23 at.% Nb [9] which is lower than its stoichiometric composition 25 at.% Ge. Carpenter [22] firstly found that the solid solution range of the Nb_3Ge phase extending from $NbGe_{0.15\pm0.01}$ to $NbGe_{0.22\pm0.01}$ at 1600 °C.

Belova and Murch [30] predicted the structure of the A_3B-A15-type compound. The B atoms form a bcc lattice (the β sublattice) while the A atoms occupy the positions in the cubic faces (the α sublattice), as shown in Fig. 3a. Geller [31] observed that the lattice constant of Nb_3Ge is larger than the prediction and suggested that the deviation from stoichiometry in the Nb-rich side of the Nb_3Ge phase is caused by the replacement of Ge atoms with Nb atoms in the β sublattice. Manning [32] suggested that the thermal vacancies are not stable in the β sublattice and there formed a quintuple defect consisting of four vacancies and an antistructure atom. In the present optimization, considering the vacancies and the antistructure atoms in the β sublattice of the A_3B-A15 structure, the two-sublattice model $(Nb)_{0.75}(Nb,Ge,Va)_{0.25}$ is used to describe the Nb_3Ge phase.

$$\begin{aligned} G_m^{(Nb_3Ge)} = {} & y^{II}_{Ge} {}^{0}G^{(Nb_3Ge)}_{Nb:Ge} + y^{II}_{Nb} {}^{0}G^{(Nb_3Ge)}_{Nb:Nb} + y^{II}_{Va} {}^{0}G^{(Nb_3Ge)}_{Nb:Va} \\ & + 0.25RT(y^{II}_{Ge} \ln y^{II}_{Ge} + y^{II}_{Nb} \ln y^{II}_{Nb} + y^{II}_{Va} \ln y^{II}_{Va}) \\ & + \sum_{n} y^{II}_{Ge} y^{II}_{Nb} {}^{n}L^{(Nb_3Ge)}_{Nb:Ge,Nb} + \sum_{n} y^{II}_{Ge} y^{II}_{Va} {}^{n}L^{(Nb_3Ge)}_{Nb:Ge,Va} \\ & + \sum_{n} y^{II}_{Nb} y^{II}_{Va} {}^{n}L^{(Nb_3Ge)}_{Nb:Nb,Va} \end{aligned} \qquad (14)$$

where y^{II}_i is the molar fraction of the element i (i = Ge, Nb, Va) in the 2nd sublattice; ${}^{0}G^{(Nb_3Ge)}_{Nb:A}$ (A = Ge, Nb, Va) the Gibbs free energy of the hypothetical compound $Nb_{0.75}A_{0.25}$; ${}^{n}L^{(Nb_3Ge)}_{Nb:i,j}$ (i, j = Ge, Nb, Va with $i \neq j$ and $n = 0, 1, 2, \ldots$) the interaction parameter between the components i and j in the second sublattice while the first sublattice is occupied by Nb atoms.

3.3.4. ($NbGe_2$) phase

The ($NbGe_2$) phase is of the $CrSi_2$-type (C40) structure. Since the homogeneity range 65.5–67.4 at.% Ge of the ($NbGe_2$) phase spans both sides of the stoichiometric composition [11], a two-sublattice model $(Ge,Nb\%)_{0.333}(Ge\%,Nb)_{0.667}$ is used to describe its Gibbs free

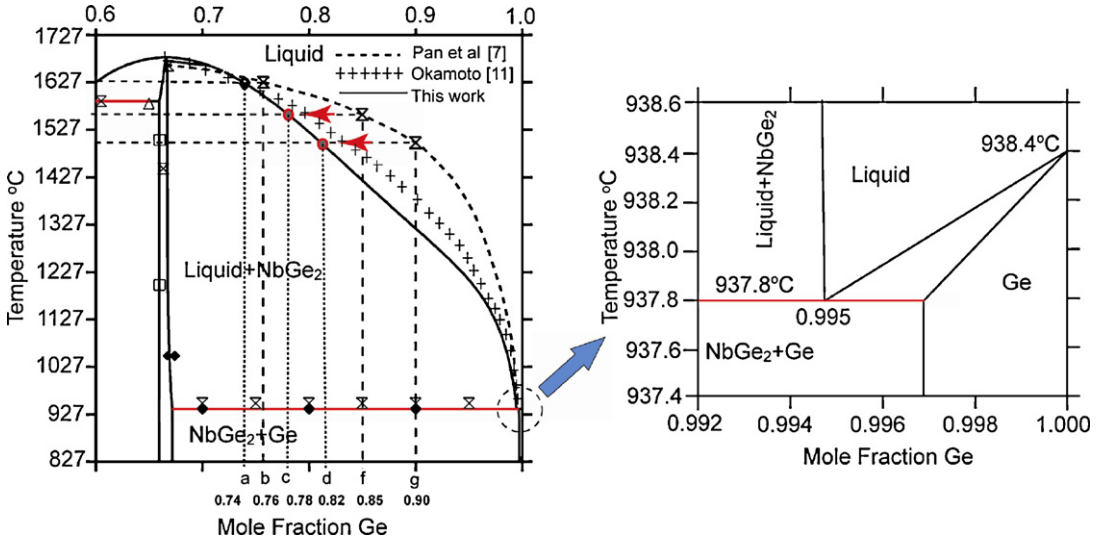

Fig. 5. The partial enlarged Ge-rich phase diagram with the composition range from 0.6 to 1.0 at.% Ge and temperature range from 827 to 1727 °C.

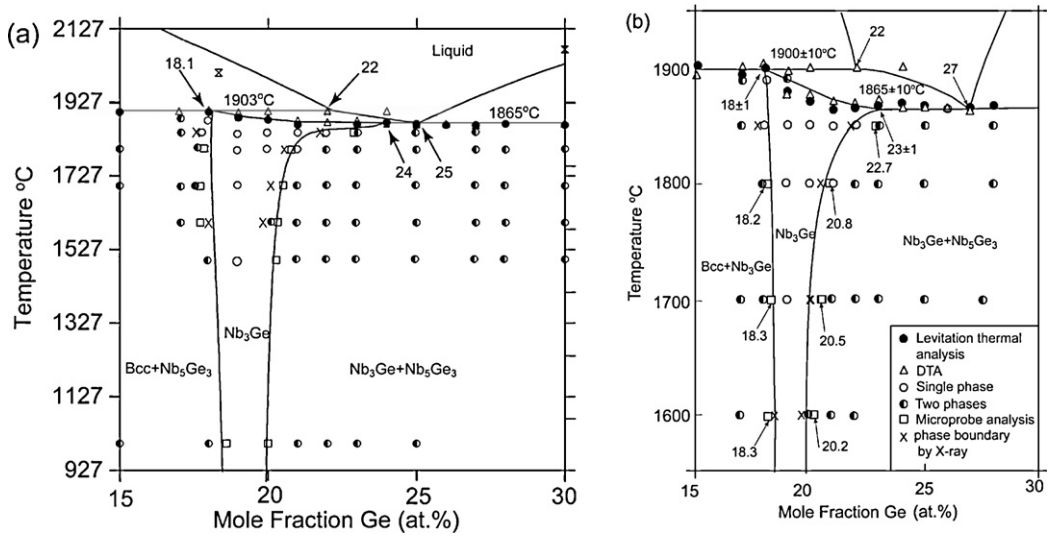

Fig. 6. The partial enlarged phase diagram of the Nb–Ge system around the Nb_3Ge phase compared with the experimental data. (a) Optimized by the present work with the temperature range from 927 to 2127 °C; (b) evaluated by Jorda et al. [9] with the temperature range from 1550 to 1950 °C.

energy expression, as follows:

$$\begin{aligned} G_m^{(NbGe_2)} &= y_{Ge}^{I} y_{Ge}^{II}\, {}^0G_{Ge:Ge}^{(NbGe_2)} + y_{Ge}^{I} y_{Nb}^{II}\, {}^0G_{Ge:Nb}^{(NbGe_2)} \\ &+ y_{Nb}^{I} y_{Ge}^{II}\, {}^0G_{Nb:Ge}^{(NbGe_2)} + y_{Nb}^{I} y_{Nb}^{II}\, {}^0G_{Nb:Nb}^{(NbGe_2)} \\ &+ 0.333RT(y_{Ge}^{I} \ \ln\ y_{Ge}^{I} + y_{Nb}^{I} \ \ln\ y_{Nb}^{I}) \\ &+ 0.667RT(y_{Ge}^{II} \ \ln\ y_{Ge}^{II} + y_{Nb}^{II} \ \ln\ y_{Nb}^{II}) \\ &+ y_{Ge}^{I} y_{Nb}^{I} y_{Ge}^{II}\, {}^0L_{Ge,Nb:Ge}^{(NbGe_2)} + y_{Ge}^{I} y_{Nb}^{I} y_{Nb}^{II}\, {}^0L_{Ge,Nb:Nb}^{(NbGe_2)} \\ &+ y_{Ge}^{I} y_{Ge}^{II} y_{Nb}^{II}\, {}^0L_{Ge:Ge,Nb}^{(NbGe_2)} + y_{Nb}^{I} y_{Ge}^{II} y_{Nb}^{II}\, {}^0L_{Nb:Ge,Nb}^{(NbGe_2)} \end{aligned} \quad (15)$$

where y_i^{I} and y_i^{II} are the site fractions of the component i (i = Nb, Ge) in the 1st and 2nd sublattices respectively; ${}^0G_{A:B}^{(NbGe_2)}$ (A, B = Nb, Ge) represents the Gibbs free energy of the hypothetical end member compound AB_2. To reduce the number of the Gibbs free energy expression, it is supposed that ${}^0L_{Ge,Nb:Ge}^{(NbGe_2)} = {}^0L_{Ge,Nb:Nb}^{(NbGe_2)}$ and ${}^0L_{Ge:Ge,Nb}^{(NbGe_2)} = {}^0L_{Nb:Ge,Nb}^{(NbGe_2)}$ in the present work.

4. Results and discussion

The optimized thermodynamic parameters are listed in Table 4. Fig. 4 shows that the calculated Nb–Ge phase diagram agrees well with the related experiment data [7–10]. The calculated results for two congruent reactions and five invariant reactions are listed in Table 1 and are compared with the experimental data. The homogeneity range (37.5–38.8 at.% Ge) of the (Nb_5Ge_3) phase at 1100 °C is consistent with the experimental data (37.9–38.5 at.% Ge) [21]. The calculated incongruent melting point (2040 °C, 41 at.% Ge) of the (Nb_3Ge_2) phase agrees well with the experimental data [7] and the calculated homogeneity range (41–42.9 at.% Ge) at 1100 °C is slightly larger than the experimental data (41.6–42 at.% Ge) [21].

The optimized liquidus is mostly consistent with the experimental data measured by Pan et al. [7] with the only large difference at the Ge-rich side since the vaporization of Ge can easily take place during the preparation process of the Nb–Ge alloys. In the Nb–Ge system, the melting point of Ge (938.3 °C) is much lower than that of Nb (2469 °C). Flukiger and Jorda [9,33] studied the experi-

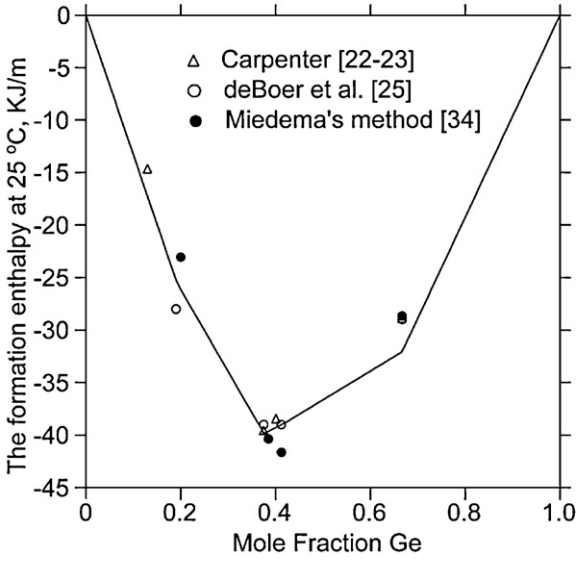

Fig. 7. The formation enthalpy of the Nb–Ge system with the experimental data at 25 °C [22,23,25,34].

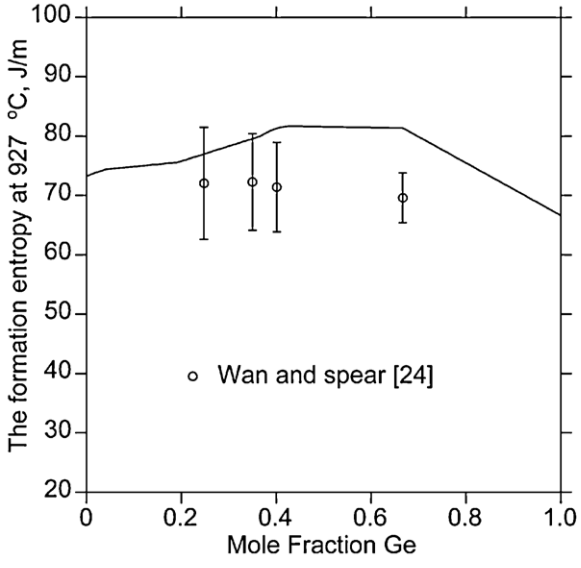

Fig. 8. The formation entropy of the Nb–Ge system with the experimental data at 927 °C [24].

Table 4
Thermodynamic parameters of the Nb–Ge system.

Phase	Sublattice model and parameters	
	GHSERNB = $-8519.353 + 142.045475T - 26.4711TLN(T)$	$298.14 < T < 2750$ K
	$+2.03475E-04T^2 - 3.5012E-07T^3 + 93{,}399T^{-1}$	$2750 < T < 6000$ K
	$-37{,}669.3 + 271.720843T - 41.77TLN(T) + 1.52824E+32T^{-9}$	
	GHSERGE = $-9486.153 + 165.635573T - 29.5337682TLN(T)$	$298.14 < T < 900$ K
	$+0.005568297T^2 - 1.513694E-06T^3 + 163{,}298T^{-1}$	$900 < T < 1211.4$ K
	$-5689.239 + 102.86087T - 19.8536239TLN(T) - 0.003672527T^2$	$1211.4 < T < 3200$
	$-9548.204 + 156.708024T - 27.6144TLN(T) - 8.59809E+28T^{-9}$	
Liquid	Model: (Ge,Nb)	$298.15 < T < 2750$ K
	${}^0G^{\text{Liquid}}_{\text{Nb}} = +29{,}781.555 - 10.816418T + \text{GHSERNB} - 3.06098E-23T^7$	$2750 < T < 6000$ K
	$-7499.398 + 260.756148T - 41.77TLN(T)$	
	${}^0G^{\text{Liquid}}_{\text{Ge}} = +37141.49 - 30.687043T + \text{GHSERGE} + 8.56632E-21T^7$	$298.14 < T < 900$ K
	$+37{,}141.489 - 30.687044T + \text{GHSERGE} + 8.56632E-21T^7$	$900 < T < 1211.4$ K
	$+27{,}243.473 + 126.324186T - 27.6144TLN(T)$	$1211.4 < T < 3200$ K
	${}^0L^{\text{Liquid}}_{\text{Ge,Nb}} = -171{,}008.9129 + 3.41895T$	
	${}^1L^{\text{Liquid}}_{\text{Ge,Nb}} = +46{,}134.81563 - 14.19642T$	
	${}^2L^{\text{Liquid}}_{\text{Ge,Nb}} = +20{,}671.04339 + 12.31747T$	
	${}^3L^{\text{Liquid}}_{\text{Ge,Nb}} = +4118.70195 - 5.60056T$	
Bcc	Model: (Ge,Nb%)	
	${}^0G^{\text{Bcc}}_{\text{Nb}} = +\text{GHSERNB}$	
	${}^0G^{\text{Bcc}}_{\text{Ge}} = +34100 - 23.5T + \text{GHSERGE}$	
	${}^0L^{\text{Bcc}}_{\text{Ge,Nb}} = -121000 - 2.5T$	
	${}^1L^{\text{Bcc}}_{\text{Ge,Nb}} = +30{,}000 + 6T$	
	${}^2L^{\text{Bcc}}_{\text{Ge,Nb}} = -22{,}000 + 38.0190T$	
Diamond-(Ge)	Model: (Ge%,Nb)	
	${}^0G^{\text{Diamond}}_{\text{Nb}} = +3000 + \text{GHSERNB}$	
	${}^0G^{\text{Diamond}}_{\text{Ge}} = +\text{GHSERGE}$	
	${}^0L^{\text{Diamond}}_{\text{Ge,Nb}} = -85{,}000 - 2T$	
Nb_3Ge	Model: $(Nb)_{0.75}(Ge\%, Nb, Va)_{0.25}$	
	${}^0G^{\text{Nb}_3\text{Ge}}_{\text{Nb:Ge}} = +0.75\ \ \text{GHSERNB} + 0.25\ \ \text{GHSERGE} - 22{,}774.7414 - 8.86092T$	
	${}^0G^{\text{Nb}_3\text{Ge}}_{\text{Nb,Nb}} = +\text{GHSERNB} + 40{,}653.1191 - 1.86845T$	
	${}^0G^{\text{Nb}_3\text{Ge}}_{\text{Nb,Va}} = +0.75\ \ \text{GHSERNB} + 61{,}452.3923 - 1.39168T$	
	${}^0L^{\text{Nb}_3\text{Ge}}_{\text{Nb:Ge,Nb}} = -73{,}741.4883 + 6.50779T$	
	${}^1L^{\text{Nb}_3\text{Ge}}_{\text{Nb:Ge,Nb}} = -44{,}203.9716 + 37.37120T$	
	${}^0L^{\text{Nb}_3\text{Ge}}_{\text{Nb:Ge,Va}} = +1844.72216 - 12.44141T$	
	${}^1L^{\text{Nb}_3\text{Ge}}_{\text{Nb:Ge,Va}} = +60{,}030 - 17.000T$	
	${}^0L^{\text{Nb}_3\text{Ge}}_{\text{Nb:Nb,Va}} = -20{,}000$	
Nb_5Ge_3	Model: $(Nb)_{0.5}(Ge,Nb\%)_{0.125}(Ge\%,Va)_{0.375}$	
	${}^0G^{\text{Nb}_5\text{Ge}_3}_{\text{Nb:Nb:Ge}} = +0.625\ \ \text{GHSERNB} + 0.375\ \ \text{GHSERGE} - 39{,}803.98 - 9.408T$	
	${}^0G^{\text{Nb}_5\text{Ge}_3}_{\text{Nb:Ge:Ge}} = +0.5\ \ \text{GHSERNB} + 0.5\ \ \text{GHSERGE} - 6000 - 14.8T$	
	${}^0G^{\text{Nb}_5\text{Ge}_3}_{\text{Nb:Ge:Va}} = +0.5\ \ \text{GHSERNB} + 0.125\ \ \text{GHSERGE} - 14{,}746.53067 - 1.60303T$	
	${}^0G^{\text{Nb}_5\text{Ge}_3}_{\text{Nb:Nb:Va}} = +0.625\ \ \text{GHSERNB} + 45{,}555.22816 - 7.08211T$	
	${}^0L^{\text{Nb}_5\text{Ge}_3}_{\text{Nb:Ge,Nb:Ge}} = {}^0L^{\text{Nb}_5\text{Ge}_3}_{\text{Nb:Ge,Nb:Va}} = -34{,}356.63405 + 0.60585T$	
	${}^0L^{\text{Nb}_5\text{Ge}_3}_{\text{Nb:Nb:Ge,Va}} = {}^0L^{\text{Nb}_5\text{Ge}_3}_{\text{Nb:Ge:Ge,Va}} = -8591.58946 - 1.0001T$	
Nb_3Ge_2	Model: $(Ge,Nb\%)_{0.222}(Ge\%,Nb)_{0.333}(Nb)_{0.333}(Ge,Va)_{0.111}$	
	${}^0G^{\text{Nb}_3\text{Ge}_2}_{\text{Nb:Nb:Nb:Ge}} = +0.888\ \ \text{GHSERNB} + 0.111\ \ \text{GHSERGE}$	
	${}^0G^{\text{Nb}_3\text{Ge}_2}_{\text{Nb:Nb:Nb:Va}} = +0.888\ \ \text{GHSERNB} + 34{,}272.70687 + 7.93092T$	
	${}^0G^{\text{Nb}_3\text{Ge}_2}_{\text{Nb:Ge:Nb:Ge}} = +0.555\ \ \text{GHSERNB} + 0.444\ \ \text{GHSERGE}$	
	${}^0G^{\text{Nb}_3\text{Ge}_2}_{\text{Nb:Ge:Nb:Va}} = +0.555\ \ \text{GHSERNB} + 0.333\ \ \text{GHSERGE}$	
	${}^0G^{\text{Nb}_3\text{Ge}_2}_{\text{Ge:Nb:Nb:Ge}} = +0.666\ \ \text{GHSERNB} + 0.333\ \ \text{GHSERGE}$	
	${}^0G^{\text{Nb}_3\text{Ge}_2}_{\text{Ge:Nb:Nb:Va}} = +0.666\ \ \text{GHSERNB} + 0.222\ \ \text{GHSERGE} - 22{,}500 + 3T$	
	${}^0G^{\text{Nb}_3\text{Ge}_2}_{\text{Ge:Ge:Nb:Ge}} = +0.333\ \ \text{GHSERNB} + 0.666\ \ \text{GHSERGE} + 20{,}537.39061$	
	${}^0G^{\text{Nb}_3\text{Ge}_2}_{\text{Ge:Ge:Nb:Va}} = +0.333\ \ \text{GHSERNB} + 0.555\ \ \text{GHSERGE} - 8250 + 1.9T$	
	${}^0L^{\text{Nb}_3\text{Ge}_2}_{\text{Ge,Nb:Ge:Nb:Va}} = {}^0L^{\text{Nb}_3\text{Ge}_2}_{\text{Ge,Nb:Nb:Nb:Va}} = 4193.99872 - 3.70905T$	
	${}^0L^{\text{Nb}_3\text{Ge}_2}_{\text{Nb:Ge,Nb:Nb:Ge}} = {}^0L^{\text{Nb}_3\text{Ge}_2}_{\text{Ge:Ge,Nb:Nb:Ge}} = -74{,}400 - 42.522T$	
	${}^0L^{\text{Nb}_3\text{Ge}_2}_{\text{Ge,Nb:Ge:Nb:Ge}} = {}^0L^{\text{Nb}_3\text{Ge}_2}_{\text{Ge,Nb:Nb:Nb:Ge}} = 0$	
	${}^0L^{\text{Nb}_3\text{Ge}_2}_{\text{Nb:Ge,Nb:Nb:Va}} = {}^0L^{\text{Nb}_3\text{Ge}_2}_{\text{Ge:Ge,Nb:Nb:Va}} = 0$	
	${}^0L^{\text{Nb}_3\text{Ge}_2}_{\text{Nb:Nb:Nb:Ge,Va}} = {}^0L^{\text{Nb}_3\text{Ge}_2}_{\text{Ge:Nb:Nb:Ge,Va}} = 0$	
	${}^0L^{\text{Nb}_3\text{Ge}_2}_{\text{Nb:Ge:Nb:Ge,Va}} = {}^0L^{\text{Nb}_3\text{Ge}_2}_{\text{Ge:Ge:Nb:Ge,Va}} = 0$	

Table 4 (*Continued*)

Phase	Sublattice model and parameters
$NbGe_2$	Model: $(Ge,Nb\%)_{0.333}(Ge\%,Nb)_{0.667}$ ${}^0G^{NbGe_2}_{Nb:Nb} = +GHSERNB + 29,469.09156 - 7.95266T$ ${}^0G^{NbGe_2}_{Nb:Ge} = +0.333\ \ GHSERNB + 0.667\ \ GHSERGE - 32,063.206 - 12.545T$ ${}^0G^{NbGe_2}_{Ge:Nb} = +0.667\ \ GHSERNB + 0.333\ \ GHSERGE - 5375.94182 + 3.05116T$ ${}^0G^{NbGe_2}_{Ge:Ge} = +GHSERGE + 18,623.70942 + 4.83337T$ ${}^0L^{NbGe_2}_{Ge,Nb:Ge} = {}^0L^{NbGe_2}_{Ge,Nb:Nb} = -19,200 + 7T$ ${}^0L^{NbGe_2}_{Nb:Ge,Nb} = {}^0L^{NbGe_2}_{Ge:Ge,Nb} = -81,400 + 25T$

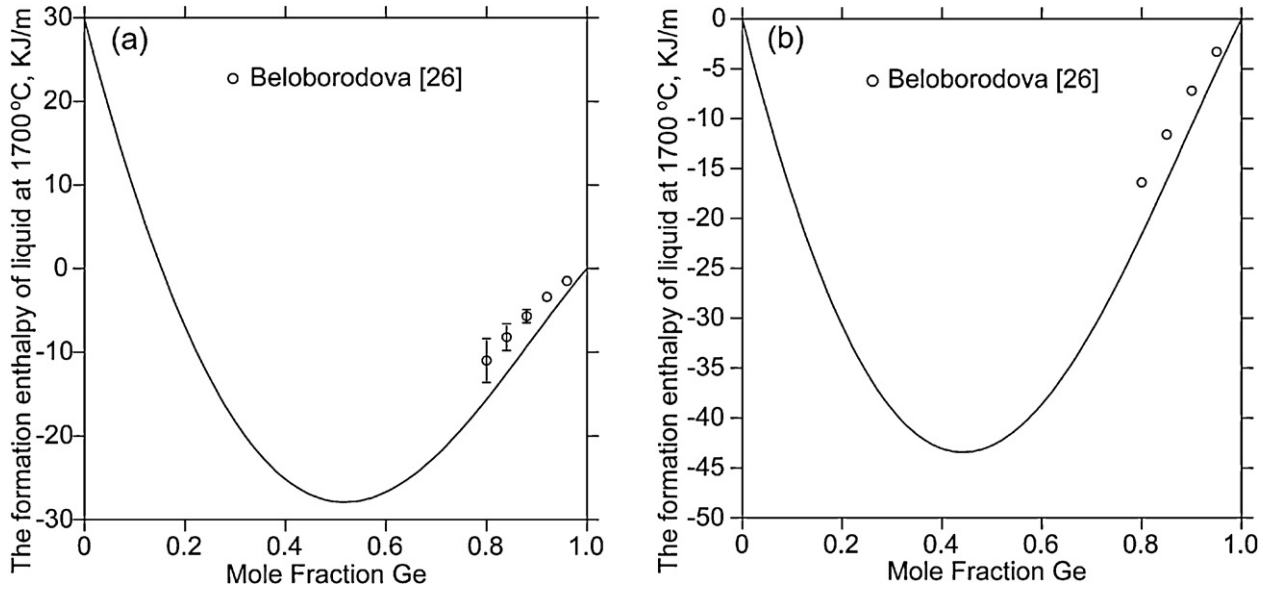

Fig. 9. The formation enthalpy of liquid with the experimental data at 1700 °C [26]. (a) The reference states are Bcc Nb and liquid Ge; (b) the reference states are liquid Nb and liquid Ge.

mental technique in the Nb–Ge phase diagram determination and concluded the weight losses became important and should be compensated for Ge concentrations higher than 30 at.% due only to the vaporization of Ge. Richter et al. [21] also studied the Nb–Ge alloys and showed the great influence of Ge evaporation during heat treatment. Annealing of Nb_3Ge_2 under dynamic vacuum will always lead to a shift of composition towards the Ge-poor tetragonal Nb_5Ge_3 and ultimately to the complete disappearance of Nb_3Ge_2.

The losses of Ge gave rise to the shifts of the overall compositions towards the Ge-poor direction. From those experimental results [9,21,33], the volatilization of Ge is more and more serious with increasing Ge concentration and the measured liquidus is more and

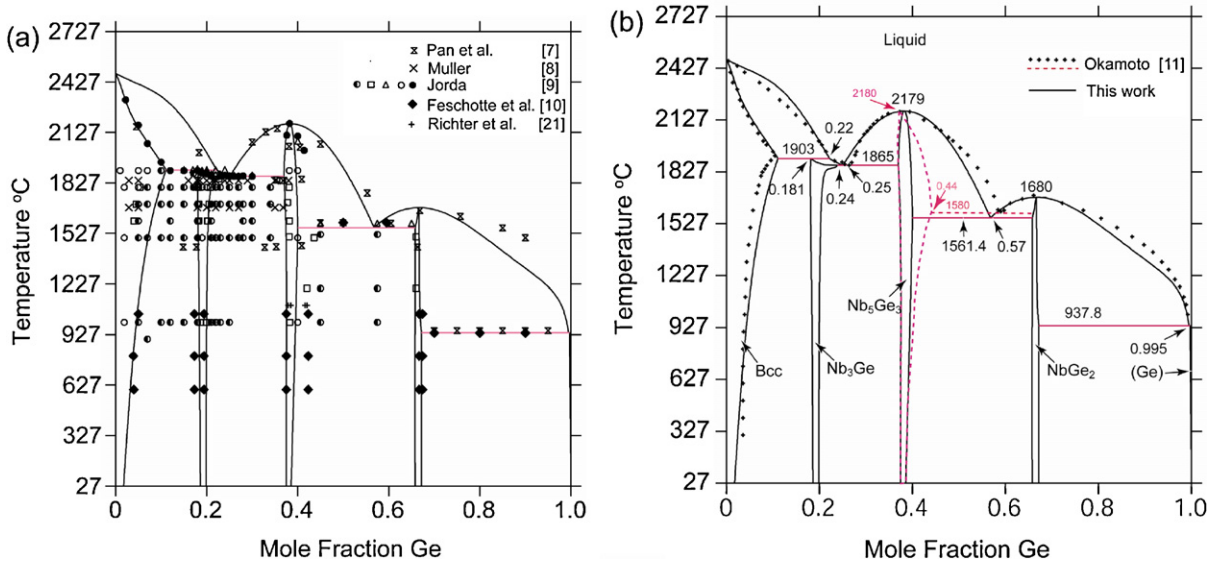

Fig. 10. The calculated Nb–Ge phase diagram without the existence of the phase Nb_3Ge_2. (a) Calculated phase diagram compared with experimental data; (b) calculated phase diagram compared with the evaluated phase diagram by Okamoto [11].

more higher than the real one. Fig. 5 shows the enlarged phase diagram at the Ge-rich side. The measured melting temperatures of the three samples at the Ge-rich side need to be revised towards the reduced Ge composition, as indicated by the arrows in the diagram. The optimized liquidus at the Ge-rich side approximates to the evaluated liquidus by Okamoto [11]. The optimized eutectic reaction at (99.5 at.% Ge, 937.8 °C) agrees with the experimental data measured by Feschotte et al. [10].

The optimized Nb_3Ge phase, Fig. 6a, is well consistent with the experimental data measured by Jorda [9], Fig. 6b.

Fig. 7 shows the formation enthalpy of the Nb–Ge system at 25 °C compared with the experimental data [22,23], the theoretical data [25] and the predicted values using Miedema's model [34]. Fig. 8 is the formation entropy of the Nb–Ge system at 927 °C compared with the experimental data estimated by Wan and Spear [24]. Fig. 9 shows the formation enthalpies of liquid with the different reference states at 1700 °C compared with the experimental data by Beloborodova [26] respectively.

Considering the arguments on whether the Nb_3Ge_2 phase can exist or not as a stable phase in the Nb–Ge phase diagram, as mentioned in Section 2.2, Fig. 10 shows the calculated phase diagram without the existence of the Nb_3Ge_2 phase. The comparisons with the experiment data, Fig. 10a, and with the evaluated phase diagram by Okamoto [11], Fig. 10b, are illustrated. Except for the obvious difference of the solubility of Nb_5Ge_3 at high temperature, the optimized phase diagram agrees well with the experiments and the evaluation.

5. Conclusions

The equilibrium relations and the thermodynamic descriptions of the phases of the Nb–Ge system were critically evaluated according to the experimental information available. The Nb_3Ge_2 phase was considered and optimized as a stable phase based on the newly reported experimental data. Different sublattice models were successfully used to describe the Gibbs free energies of the phases. The experimental data of the phase equilibria, the formation enthalpy and the formation entropy were used to optimize the parameters of the Gibbs free energy expressions. Considering the influence of the Ge volatilization on the measured liquidus temperature, the present optimized thermodynamic data can be used to reproduce the experimental data well.

Acknowledgements

Thanks to the Royal Institute of Technology, Sweden for supplying the Thermo-Calc software. This work was supported by the National Natural Science Foundation of China (No. 50671009 and 50731002) and the National Doctorate Fund of the State Education Ministry of China (No. 20060008015).

References

[1] L. Li, B.R. Zhao, P. Zhou, S.Q. Guo, Y.X. Zhao, Journal of Low Temperature Physics 45 (3–4) (1981) 287–294.
[2] Y. Nakagawa, M. Umeda, Journal of Applied Physics 75 (4) (1994) 2131–2140.
[3] M. Suzuki, Y. Watanabe, T. Anayama, K. Watanabe, K. Noto, Japanese Journal of Applied Physics 26 (6) (1987) 881–885 (Part 1 (Regular Papers & Short Notes)).
[4] K.E. Kihlstrom, P.D. Hovda, V.Z. Kresin, S.A. Wolf, Physical Review B: Condensed Matter 38 (7) (1988) 4588–4591.
[5] E.P. George, M. Yamaguchi, K.S. Kumar, C.T. Liu, Annual Review of Materials Science 24 (1994) 409–451.
[6] C.T. Liu, J. Stringer, J.N. Mundy, L.L. Horton, P. Angelini, Intermetallics 5 (8) (1997) 579–596.
[7] V.M. Pan, V.I. Latysheva, E.A. Shishkin, Physics and Metallurgy of Superconductors (1970) 179–182.
[8] A. Muller, Zeitschrift fur Naturforschung A (Astrophysik, Physik und Physikalische Chemie) 25 (11) (1970) 1659–1669 (in German).
[9] J.L. Jorda, R. Flukiger, J. Muller, Journal of the Less-Common Metals 63 (1978) 25–37.
[10] P. Feschotte, A. Polikar, G. Burri, Comptes Rendus Hebdomadaires des Seances de l'Academie de Sciences Serie C (Sciences Chimiques) 288 (3) (1979) 125–128 (in French).
[11] H. Okamoto, in: H. Okamoto (Ed.), Phase Diagrams for Binary Alloys, ASM International, Materials Park, OH 44073-0002, 2000, pp. 3359–3360.
[12] P. Villars, L.D. Calvert, Pearson's Handbook of Crystallographic Data for Intermetallic Phases, ASM International, Metals Park, OH, 1991.
[13] H. Nowotny, in: P.A. Beck (Ed.), Electronic Structure and Alloy Chemistry of the Transition Elements, Plenum Press, New York, 1963, p. 179.
[14] J.J. Williams, Y.Y. Ye, M.J. Kramer, K.M. Ho, L. Hong, C.L. Fu, S.K. Malik, Intermetallics 8 (8) (2000) 937–943.
[15] A.J. Thom, V.G. Young, M. Akinc, Journal of Alloys and Compounds 296 (1–2) (2000) 59–66.
[16] J.D. Corbett, E. Garcia, A.M. Guloy, W.-M. Hurng, Y.-U. Kwon, A.E. Leon-Escamilla, Chemistry of Materials 10 (10) (1998) 2824–2836.
[17] H. Nowotny, A.W. Ssercy, J.E. Orr, Journal of Physical Chemistry 60 (1956) 677–678.
[18] A.I. Braginski, G.W. Roland, M.R. Daniel, Applied Polymer Symposia 29 (1975) 93–104.
[19] Y. Iijima, T. Igarashi, K. Hirano, Journal of Materials Science 14 (2) (1979) 474–479.
[20] M. Kloska, E.L. Haase, Journal of the Less-Common Metals 99 (2) (1984) 241–248.
[21] K.W. Richter, H. Flandorfer, H.F. Franzen, Journal of Alloys and Compounds 320 (1) (2001) 87–92.
[22] J.H. Carpenter, Journal of Physical Chemistry 67 (1963) 2141–2144.
[23] J.H. Carpenter, A.W. Searcy, Journal of Physical Chemistry 67 (1963) 2144–2147.
[24] C.F. Wan, K.E. Spear, Electrochemical Society 77 (5) (1977) 47–58.
[25] F.R. deBoer, R. Boom, W.C.M. Mattens, A.R. Miedema, A.K. Niessen, Cohesion in Metals. Transition Metal Alloys, 1988 (North-Holland, Amsterdam, Netherlands).
[26] E.A. Beloborodova, Poroshkovaya Metallurgiya 7–8 (1996) 76–79 (in Russian).
[27] A.T. Dinsdale, CALPHAD 15 (4) (1991) 317–425.
[28] H.J. Seifert, H.L. Lukas, G. Petzow, Zeitschrift fur Metallkunde 87 (1) (1996) 2–13.
[29] P.B. Fernandes, G.C. Coelho, F. Ferreira, C.A. Nunes, B. Sundman, Intermetallics 10 (10) (2002) 993–999.
[30] I.V. Belova, G.E. Murch, Journal of Physics and Chemistry of Solids 58 (9) (1997) 1383–1390.
[31] S. Geller, Acta Crystallographica 9 (1956) 885–889.
[32] J.R. Manning, American Journal of Physics 36 (10) (1968) 922–923.
[33] R. Flukiger, J.L. Jorda, Applications of Phase Diagrams in Metallurgy and Ceramics, 1978, pp. 375–406.
[34] X.Q. Chen, R. Podloucky, CALPHAD 30 (3) (2006) 266–269.